Escola de Primavera de Transição e Turbulência
Blumenau 2020

ABCM Associação Brasileira de Engenharia e Ciências Mecânicas

12th Spring School on Transition and Turbulence
September 21st-25th, 2020, Blumenau, SC, Brazil

EPTT-2020-0101
COMPENSATION OF IMAGE DISTORTION ON PIV MEASUREMENTS OF A STIRRED TANK

Aliandra D. Barbutti
Process Engineering Department, University of Campinas, School of Chemical Engineering.
a115976@dac.unicamp.br

Aline G. De Mitri
Process Engineering Department, University of Campinas, School of Chemical Engineering.
a093335@dac.unicamp.br

Jenniffer S. Ayala
Process Engineering Department, University of Campinas, School of Chemical Engineering.
J192526@dac.unicamp.br

Rodrigo de L. Amaral
NDF, Department of Mechanical Engineering, POLI, University of São Paulo
rodrigoamaral@usp.br

Helder L. de Moura
Process Engineering Department, University of Campinas, School of Chemical Engineering.
helderlima@feq.unicamp.br

José R. Nunhez
Process Engineering Department, University of Campinas, School of Chemical Engineering.
nunhez@unicamp.br

Guilherme J. de Castilho
Process Engineering Department, University of Campinas, School of Chemical Engineering.
guijcas@unicamp.br

Abstract. *Particle image velocimetry (PIV) measurements are increasingly common in the investigation of turbulent flow parameters for the optimization of stirred tanks. Generally, PIV applications are performed using the camera's position perpendicular to the light plane. In some cases, the use of tilted images is the most suitable when optical access is limited. In addition, the curvature of the tank also changes the relationship between the physical space and the image plane, causing distortions. These can be compensated in the physical space using a wedge around the tank, for example, but it is often expensive or unfeasible in the experimental arrangement. In the image plane, a third-order polynomial function can be used to correct the distortion effect from a calibration procedure. However, this global function could fail in regions with high distortions. This work aims to investigate the performance of the image distortion compensation on PIV measurements of a stirred tank without a wedge around it. Two cameras with different positions were used to simultaneously record a calibration target, in order to obtain a polynomial function from a calibration procedure in one and two steps (multicalibration). This approach has shown promising for the camera positioned with the smallest angular displacement in relation to the object plane. The best configuration was then applied to evaluate turbulent kinetic energy (TKE) distribution. However, the calibration and the multicalibration did not present significant differences, and both were considered adequate in the analysis of stirred tanks.*

Keywords: *image distortion compensation, stirred tank, PIV*

1. INTRODUCTION

Stirred tanks are widely used for various industrial applications involving heat, moment, and mass transfer operations. The equipment geometry, number of baffles, model and arrangement of the impeller are characteristics that influence the turbulent flow pattern inside the vessel. (Alonzo-Garcia *et al.*, 2019). Pharmaceutical industries, for example, have used mechanically agitated high-throughput experimentation (HTE) reactors to develop catalysts for polymerization reactions. These reactors are small-scale, and if associated with low Reynolds numbers can have low mixing efficiency and limited

mass transfer rate. A more detailed understanding of the hydrodynamics and the mixing pattern inside these reactors is essential to optimize their operation and thus maximize the efficiency of the formulations (Chung *et al.*, 2009). Moreover, in the petrochemical industry, stirred tanks with side-entering agitators are used to store crude oil and fuels such as gasoline and diesel to guarantee the homogenization of the liquid mixture. In these situations, the mixing parameters are often determined in a heuristic manner as there are few studies involving their evaluations, even on a laboratory scale. (Fang *et al.*, 2011; Gómez *et al.*, 2010). In order to fully comprehend these mixing mechanisms in stirred tanks, it is necessary to detail their hydrodynamics. For instance, the size and periodicity of eddies and vortices formed by agitation influence the mixing models and parameters, especially the turbulent kinetic energy and energy dissipation rate (Kresta and Wood, 1991).

Flow parameters analyzed in a stirred tank can be the instantaneous and average velocities, the periodically induced stress, the mixing efficiency, the mass transfer and its interactions, and the Reynolds stress. These support the identification and quantification of the kinetic energy transfer between the mean flow and the periodic and turbulent fluctuations (de Lamotte *et al.*, 2017; Escudié and Liné, 2003). They also allow the estimation of the turbulent kinetic energy (TKE) and the energy dissipation rate (EDR), which are essential characteristics for stirred tank designs. Regarding TKE, the velocity fluctuations are related to turbulent dispersion and mixing, as well as the impeller geometry, position in the tank, and the rotation speed influence the mixture quality, particularly in regions close to the tank's wall and near the impeller blades where eddies are formed.

The identification of turbulent flow parameters requires instantaneous information of the velocity field in axial, radial, and tangential directions (Khan *et al.*, 2006). Different experimental techniques can be applied, for example, particle image velocimetry (PIV), which also allows quantifying the characteristic eddies scales and evaluating the mixing processes (Alonzo-Garcia *et al.*, 2019; de Lamotte *et al.*, 2017). PIV is a quantitative and non-intrusive technique capable of determining velocity fields by the analyzes of tracer particle images. The measurement principle consists of a laser system that illuminates the flow region of interest and interacts with the particles immersed in the fluid to allow the acquisition of images every two consecutive times by cameras usually positioned at 90º of the light sheet. The determination of the speed field is carried out through the analysis of cross-correlation between the particle images in small areas known as interrogation windows. Hence, this method reconciles the use of high-resolution cameras and powerful lasers that can register all points of a velocity field in flow even in turbulent regimes. (Adrian and Westerweel, 2011; Raffel *et al.*, 2018; Bernhard Wieneke, 2017).

The quality of PIV measurements is directly related to the precision in which the displacements of the particle images can be measured, and thus represent the average displacement of the particle population in an interrogation window. Image distortion is an effect that can deteriorate the quality of these measurements, as it creates a non-linear relationship between the particle's position in physical space and its corresponding image. It occurs when any source promotes variation in the magnification as a function of the particle image's position in the plane. Magnification is the ratio between the distance of the image and the object to the center of the lens. The leading causes of the magnification variation in the images are imperfections in the lens design, misalignment of the image recording plane with the object plane, and refraction. The distortion associated with the heterogeneity of refraction is evidenced by the curvature of the investigation region (tank, bubble column, pipe) and differences in the refractive index of the fluid and the equipment material. The curvature can act as an optical lens and blur the recorded image. These variations cause systematic errors concerning the velocity and the position of the vector in the image plane; however, these can redress from experimental calibration or distortion compensation algorithms (Elsinga *et al.*, 2005; Raffel *et al.*, 2018; Soloff *et al.*, 1997)

In order to compensate image distortions, two different approaches can be applied. The first is to reduce the interference in the physical space by changing the physical structure of the experimental system. Straight-walled wedges can be adapted to reduce the effects of the tank's curvature and ensure an orthogonal position of the cameras' line of sight. For better performance of the wedges, they must have thin walls, be produced with the same transparent material as the structure of the experiment (glass or acrylic, for example), and be filled with the same liquid of the main flow (Prasad and Jensen, 1995). Sharp and Adrian (2001) applied a rectangular wedge to assess the turbulent structures in a cylindrical tank agitated by Rushton impellers. At the same time, Micheletti *et al.* (2004) encased the tank with a square trough to carry out Laser Doppler Anemometry (LDA) and PIV measurements to identify the energy dissipation rate of flows induced by the same type of impeller. The values obtained were compared with estimates of numerical methods and showed good agreement. Chung *et al.* (2007; 2009) inserted the experimental cylindrical tank into a cubic tank and performed PIV experiments to evaluate different arrangements: with deflectors, without deflectors, and with the impeller in an eccentric position. Both studies were able to characterize the flow periodicities and to estimate the turbulent parameters without the influence of refractive distortions. Li *et al.* (2011) employed a rectangular tank around the experimental tank with the same objective of minimizing optical refraction. The authors studied the influence of the diameter of the Rushton impeller on the turbulent flow of a stirred tank using PIV measurements at a resolved angle and Large Eddy Simulations (LES) and obtained satisfactory results for both methods. Stelmach *et al.* (2019) evaluated the distribution of turbulent kinetic energy in a tank agitated by a self-aspirating disk impeller. The study was made from PIV measurements at a resolved angle and applied a rectangular wedge around the cylindrical tank, similar to Li *et al.* (2011). In turn, Alonzo-Garcia *et al.* (2019) used PIV measurements made in a tank surrounded by a cubic wedge to validate different turbulence simulation models. Despite all these applications, the use of wedges has as main problems the

complexity of wedge construction, which makes its application often unfeasible, as well as the high cost of installation and use, especially if the fluid applied inside the structure is not water.

When physical space methods are not sufficient to eliminate optical distortions, a second approach can be applied. It refers to parameter alterations in the image plane by mapping functions used in the image reconstruction to correct such distortions if they are not so severe as to make the image of the calibration target unacceptably inaccurate. The mapping function relates to the location of the particle in the physical space with the image recording plane. Most correlation methods determine the velocity vectors in a uniform grid fixed in the pixel matrix of the image acquisition camera, and it is impossible to obtain data in a non-uniform grid. However, by using the mapping function, vectors can be interpolated in any grid within the function domain. (Adrian and Westerweel, 2011; Raffel *et al.*, 2018; Soloff *et al.*, 1997).

The mapping function is generated from a calibration procedure with a calibration target. According to Soloff *et al.* (1997), this target must be elaborated based on the system characteristics under study and is a fundamental step for a successful calibration. The calibration target must have characteristic marks, usually points, placed under an equally spaced Cartesian grid. The image of the mark pattern is responsible for defining how the positions in the object plane are mapped to the positions in the image plane. Thus, the number of points and their spacing are chosen based on the acquisition area and the distortion. The size and geometry of the target are defined and limited by the measurement medium, but they must be large enough to occupy the entire camera's field of view. Before starting the calibration procedure, it is necessary to define the origin of the coordinate system, and the other points are measured concerning this origin mark.

Based on the mapping function, it is possible to calculate the displacements of particles anywhere in the studied area. Many numerical methods can be used to obtain the mapping function; however, due to its simplicity, it is common to use a multidimensional polynomial. The relative error of the function is associated with the domain size of the mapping function in the investigated direction. It indicates the deviation among flow displacements regarding the size of the mapped region. The calibration procedure proposed by Soloff *et al.* (1997) has been applied in many studies to allow the recombination of stereoscopic images in building three-dimensional velocity fields (Alberini *et al.*, 2017; Khan *et al.*, 2006; Kilander and Rasmuson, 2005). Nevertheless, to the best of the authors' knowledge, no study of two-dimensional flow in stirred tanks has applied the calibration strategy to obtain PIV measurements, and the application of wedges are still preferred.

The present work aims to investigate the performance of the approach developed by Soloff *et al.* (1997) to compensate the image distortions of PIV measurements in a stirred tank without the use of wedges. The proposal consists of taking the measurements with the camera at an angle offset from the normal light plane, in addition to applying the calibration procedure to obtain the mapping function. The distortion compensation is then assessed through qualitative and quantitative analysis of the adjustment of the mapping function to the images of a calibration target. Besides, the influence of the approach on the distribution of the turbulent kinetic energy from the flow is verified.

2. EXPERIMENTAL

2.1 Experimental apparatus and data acquisition

A pilot unit of a stirred vessel (Fig. 1a) was used in the experiments. The acrylic cylindrical tank had inner diameter T = 380 mm and a standard torispherical base ASME 10%. The liquid was agitated by a 45° pitched blade turbine (PBT) with diameter $D = 2T/5$ e clearance $C = T/3$. The tank was equipped with four equally spaced baffles of width $B = T/10$ (Fig. 1b) and filled with water (density ρ = 997 kg/m³ and viscosity $\mu = 1{,}002.10^{-3}$ Pa.s) to a height of H = T.

In order to assess the positioning of the camera in distortion compensation, the recording was made by two cameras of the *FlowSense EO 8M-21* model (3312 x 2488 pixels, 5 Hz) in different positions (Fig 1c): camera 1 at $\sigma = 10^o$ and camera 2 at $\sigma + \beta = 40^o$ to the normal of the light sheet (object plane). Despite the unusual configuration, the Scheimpflug principle was respected, that is, the collinearity between the planes of the object, the lens, and the image was ensured to guarantee the focus on the object plane (Prasad, 2000). Figure 1d provides a more detailed view of the arrangement between cameras, laser, and stirred tank. The calibration target was a 210 mm x 750 mm plate made of ABS polymer, which was printed in a dot pattern with a diameter of 0.5 mm equally spaced at a center-to-center distance of 1.5 mm. The aperture of the lens was manually adjusted to make sure the complete image was in focus. The image acquisition was performed using the *DynamicStudio* software (Dantec Dynamics).

Figure 2 shows the raw images of the calibration target obtained by cameras 1 (Cam 1) and 2 (Cam 2). To better visualize the distortion of the images, two regions were selected and enlarged: region 1 (R1), close to the shaft, and region 2 (R2), close to the tank wall. With regard to camera 1, positioned closer to the normal axis of the calibration target, it can be seen that both regions had a negative slope in the dot pattern, this slope was $-15.29^o \pm 0.50^o$ for R1 and -20.34 ± 1.40^o for R2. However, for camera 2, positioned closer to the calibration target plane, the points on R1 were practically straight, with a slight inclination of $0.84^o \pm 0.32^o$, while R2 presented a significant positive inclination of $17.20^o \pm 0{,}55$. Although both cameras present distortions in the images, for camera 1 the whole image follows a similar pattern of variation, whereas, for camera 2, the regions have very different inclinations. In this case, the correction by the calibration procedure using a global mapping function becomes more challenging.

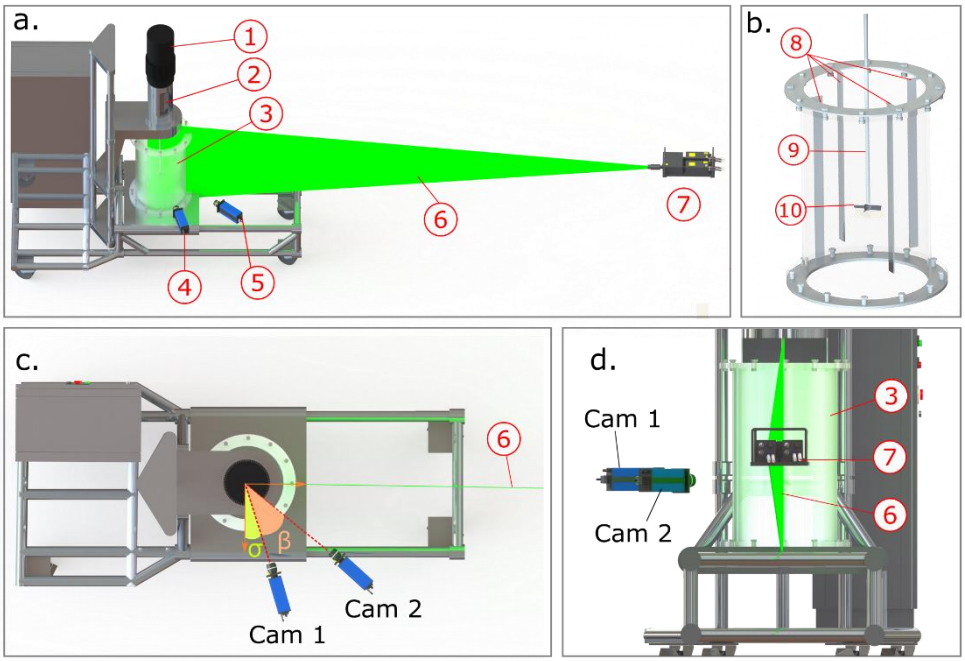

Figure 1. Experimental apparatus (a), stirred vessel (b), lateral (c) and vertical (d) field of view of the position of the cameras and the light sheet. Legend: 1. Engine, 2. Torque meter, 3. Stirred tank, 4. Camera 1, 5. Camera 2, 6. Baffles, 7. Shaft, 8. Impeller.

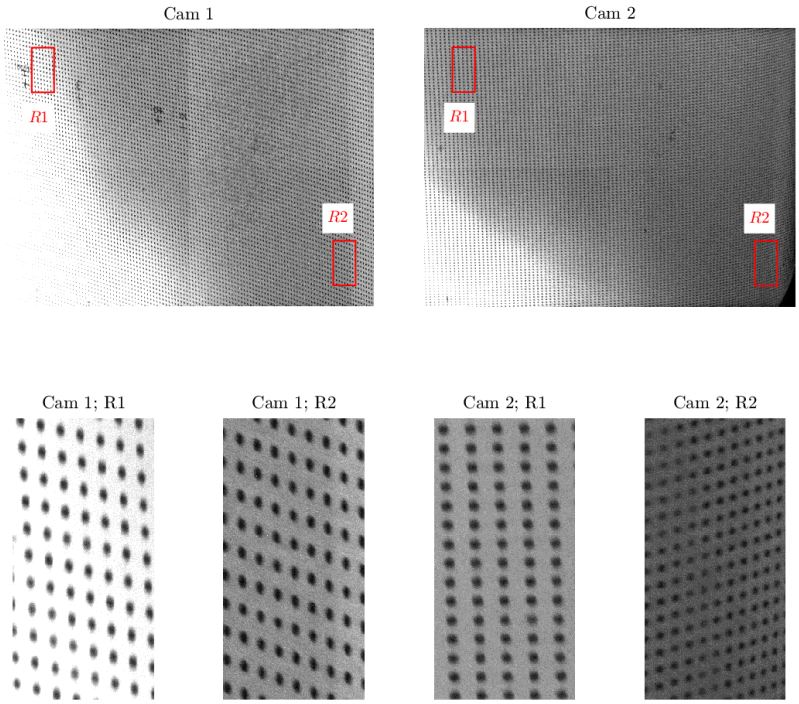

Figure 2. Raw images of the calibration target for the cameras 1 (Cam 1) and 2 (Cam 2) highlighting two regions: close o the shaft (R1) and near the tank's wall (R2).

2.2. Calibration of Soloff *et al.* (1997)

In the calibration procedure, the relationship between the physical coordinates (*X'*, *Y'*) and the image coordinates (*x*, *y*) was described by a mapping function, according to the strategy proposed by Soloff *et al.* (1997). The function was

obtained by adjusting the points identified on the target to a third-order polynomial (Eq. 1). This model was considered to be more suitable for situations with high error from a global or local perspective (B. Wieneke, 2005).

$$\begin{pmatrix} x \\ y \end{pmatrix} = \begin{bmatrix} X' + \partial X(X', Y') \\ Y' + \partial Y(X', Y') \end{bmatrix} \tag{1}$$

where $\partial X'$ e $\partial Y'$ are defined by Eq. 2:

$$\begin{pmatrix} \partial X' \\ \partial Y' \end{pmatrix} = \begin{bmatrix} a_0 + a_1 s + a_2 s^2 + a_3 s^3 + a_4 t + a_5 t^2 + a_6 t^3 + a_7 st + a_8 s^2 + a_9 s^2 \\ b_0 + b_1 s + b_2 s^2 + b_3 s^3 + b_4 t + b_5 t^2 + b_6 t^3 + b_7 st + b_8 s^2 + b_9 s^2 \end{bmatrix} \tag{2}$$

The displacements $\partial X'$e $\partial Y'$ are determined by normalized coordinates s (Eq. 3) and t (Eq. 4)

$$s = 2 \cdot (X' - X'/n_x) \tag{3}$$

$$t = 2 \cdot \left(Y' - Y'/n_y\right) \tag{4}$$

where n_x and n_y are the images' size, in pixel, X_0' and Y_0' are reference points identified in the target image. Thus, the determination of the mapping function is done by recognizing the points on the calibration target (X' and Y' values) and estimating the a_i and b_i coefficients of Eq. 2 by the method of least-squares. This procedure was performed using *Davis 8.4* software (LaVision).

The reference points X_0' and Y_0' were defined in the center of the plate's raw image. Also, a search pattern was used considering a second point and a third point spaced 1.5 mm from the reference point (Fig. 3a) to facilitate the valid identification of the pattern in the plate image (Fig. 3b). After identification, the mapping function coefficients were estimated. According to Soloff *et al.* (1997), the adjustment of the mapping function is ideal when the adjustment error is less than 1 pixel. Besides, the quality of the adjustment was analyzed by overlaying a grid with the same spacing as the calibration target with a center in X_0' and Y_0' (Fig. 3c). In this case, the mapping function was considered adequate if the grid overlapped the points on the plate image. In the reconstruction, the image was dewarped using the mapping function and a cubic interpolation.

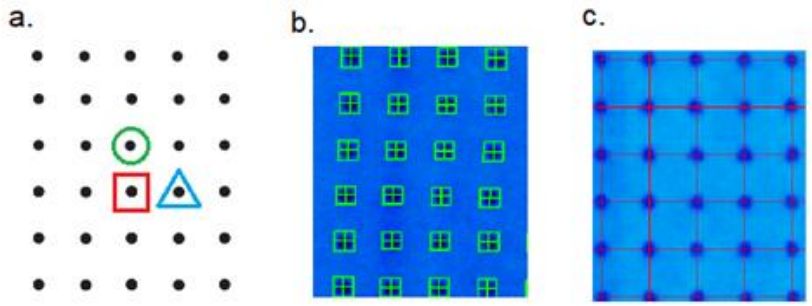

Figure 3. Basics steps of the calibration proposed by Soloff *et al.* (1997).

3. RESULTS AND DISCUSSION

3.1. Analysis of the calibration of Sollof *et al.* (1997)

The dewarped images from cameras 1 and 2 after calibration are shown in Figures 4 and 5. Three regions were analyzed in detail: close to the impeller shaft (R1), close to the impeller tip (R2) and near the tank wall (R3). The adjustment error of the global mapping function was 0.85 and 6.80 pixels for camera 1 and 2, respectively. For camera 1 (Fig. 4), the grid overlapped the target pattern of points for R1 and R2. However, the overlap failed near the tank wall (R3). The lack of adjustment on the wall can be explained mainly by the lack of identification of the plate points in this region, although approximately 9000 points were recognized in the entire image. The curvature of the wall distorted the image of the points, which appeared elongated and with variations in center-to-center spacing. This effect is even more evident in the R3 of camera 2 (Fig. 5). For this camera, besides the non-homogeneous distortion observed in Fig. 2 and the high adjustment error of the mapping function (of 6.80 pixels), the failure in the calibration can be analyzed by the lack of grid overlapping in the target pattern of points for the three regions of Fig. 5.

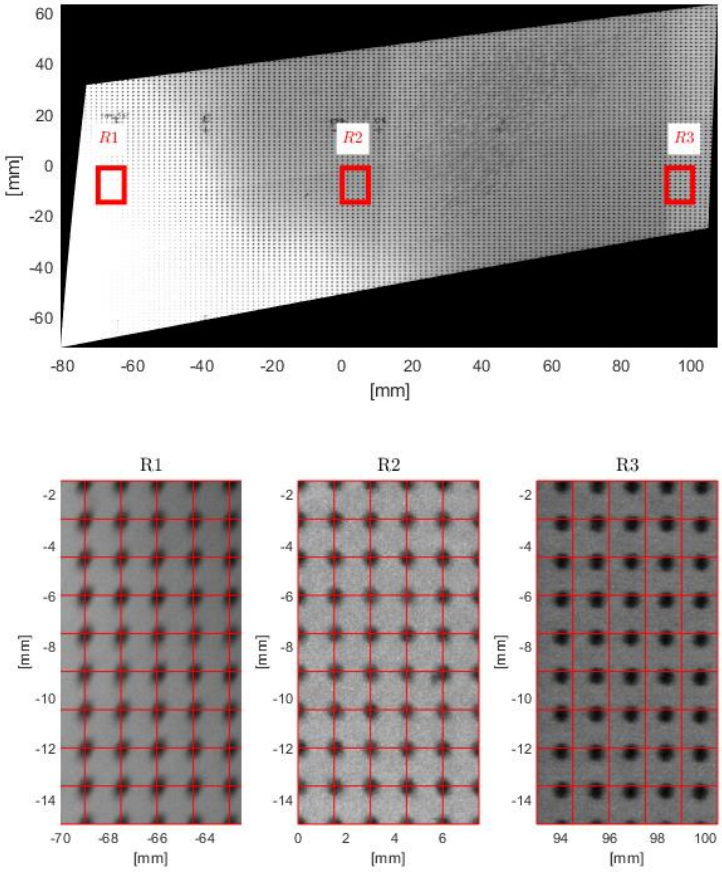

Figure 4. Dewarped image of the calibration target from camera 1 after the calibration of Soloff *et al.* (1997). Comparison among the dewarped images and the mapping function adjustment close to the impeller shaft (R1), close the impeller tip (R2) and near the tank wall (R3).

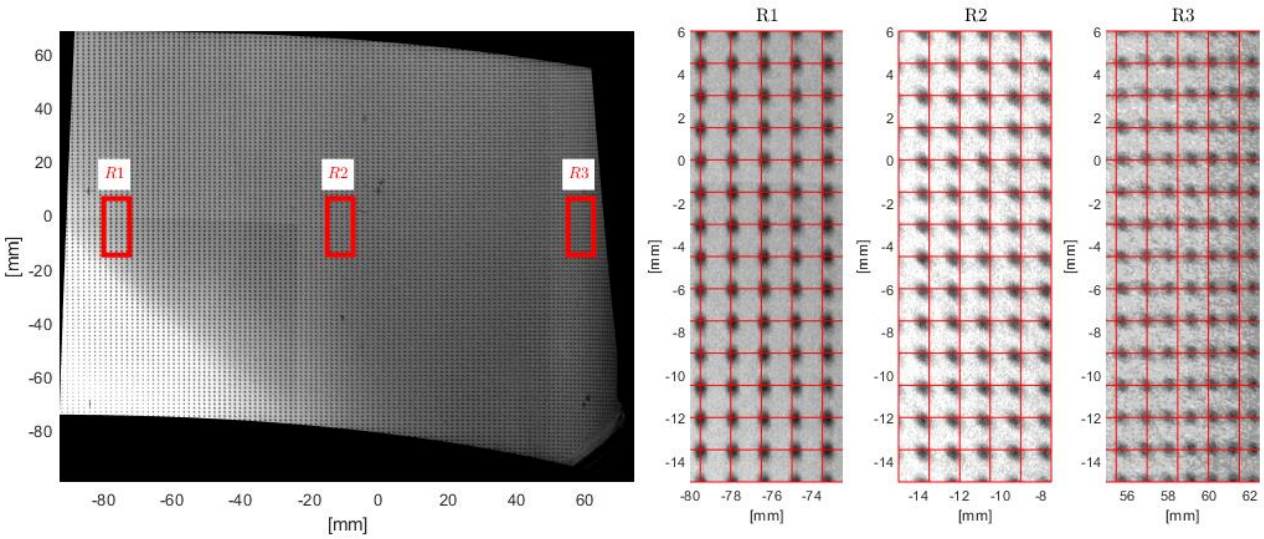

Figure 5. Dewarped image of the calibration target from camera 2 after the calibration of Soloff *et al.* (1997). Comparison among the dewarped images and the mapping function adjustment close to the impeller shaft (R1), close the impeller tip (R2) and near the tank wall (R3).

After observing the poor adjustment of the global mapping function, especially near the tank wall, it was proposed to perform a new calibration step. Figure 6 shows the multicalibration strategy implemented in this situation, also performed in the *Davis 8.4* software (LaVision). In this new stage, the dewarped images of the calibration target (Fig. 4) underwent a second calibration, in which the reference points $X'_{0,2}$ and $Y'_{0,2}$ were selected close tank wall region. To identify more points close to the wall, the point diameter was defined as 0.75 mm and the center-to-center distance was maintained at 1.5 mm. Again, the procedure for obtaining the mapping function was performed, resulting in a new reconstructed image. After this new stage, a better adjustment of the mapping function close to the wall was observed for camera 1 (Fig. 7). However, the points in the impeller shaft region (R1) were not recognized either by camera 1 image or in camera 2 image, probably due to the variation in the size of the points because of the origin selection in the region close to the wall (R3). For camera 2, the lack of adjustment observed in the first calibration was repeated in this new stage. In the second calibration, the adjustment errors were 1.24 and 9.25 pixels for cameras 1 and 2, respectively.

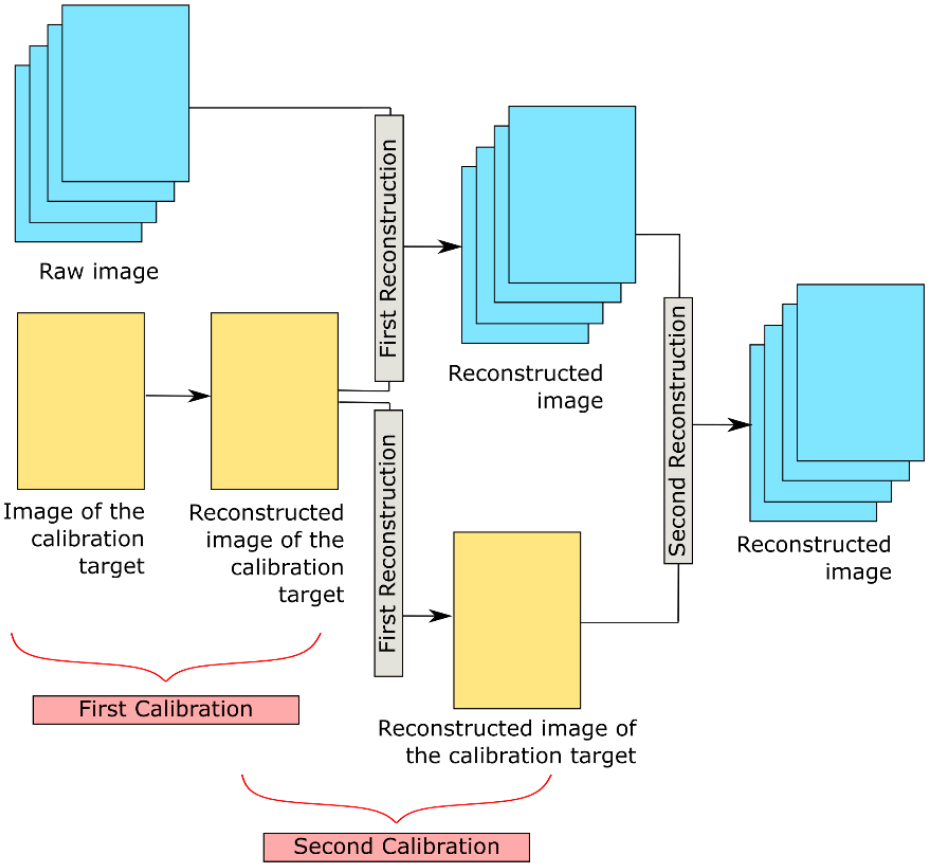

Figure 6. Multicalibration strategy.

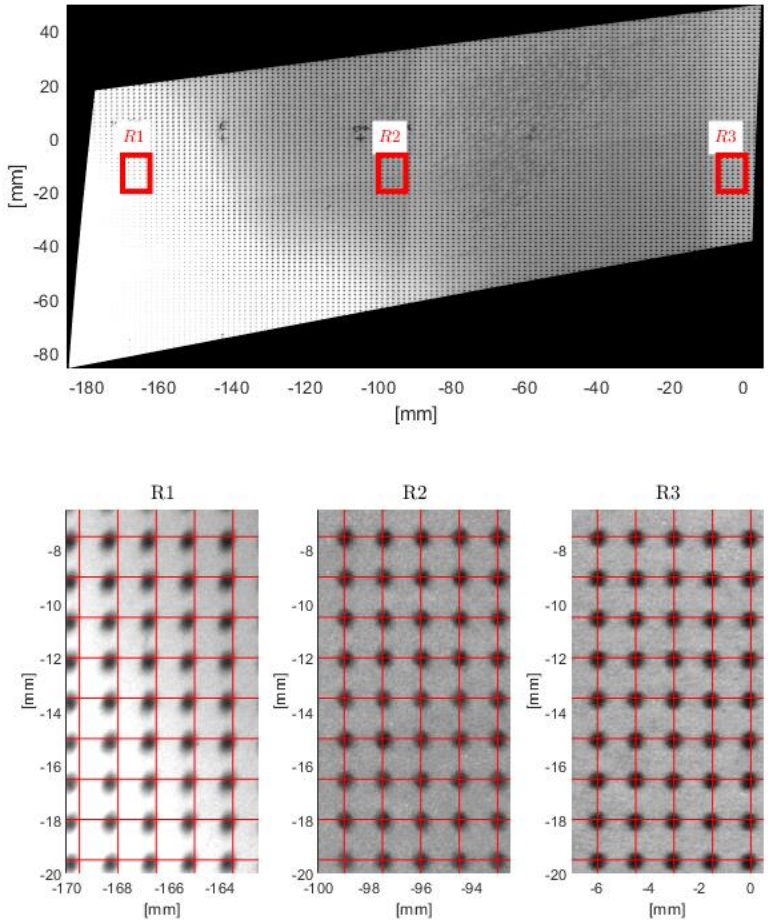

Figure 7. Dewarped image of the calibration target from camera 1 after the multicalibration. Comparison among the dewarped images and the mapping function adjustment close to the impeller shaft (R1), close the impeller tip (R2) and near the tank wall (R3).

3.3. Effect of the distortion compensation on the turbulent kinetic energy distribution (TKE)

Based on the information analyzed concerning the positioning of the cameras and the results obtained after the procedures of the first and the second calibration, it was decided to analyze the performance of the approaches in the flow only with camera 1. The PIV technique was applied in the stirred vessel described in Figure 1. The impeller speeds (660 rpm) have been chosen to achieve a turbulent regime ($Re = \rho N D^2/\mu \cong 170.000$). Images for the flow analysis were obtained using a 2D-2C PIV system (two dimensions and two components) developed by Dantec Dynamics. The total area investigated was 0.39 m x 0.19 m, and, as previously mentioned, only camera 1 was used, positioned at 40º from the normal plane of the light sheet (Fig. 1c). The light sheet with 2 mm of thickness was supplied by an *Nd: YAG* laser (532 nm, 200 mJ). As tracer particles, silver-coated hollow glass spheres with an average diameter of 10 μm and density of 1100 kg / m³, were used, since this value was close to the density of the fluid, in order to guarantee the faithful following of its flow (Raffel *et al.*, 2018). A set of 1000 pairs of images were recorded with an interframe time of 100 μs.

With the purpose to analyze the different velocity fluctuations in the turbulent flow, images at different angles resolved (AR) of the impeller shaft were acquired. The images were recorded at AR 0° with the light plane shifted about 0.5° from the baffled to minimize the effect of the structure light reflection, AR 15º, 30º, 45º, 60º and 75º. The pulsation of the laser, the recording of the cameras and the rotation of the impeller were synchronized employing a microcontroller, which received the value of the rotation speed and sent a signal of the axis revolution time to the synchronizer of the PIV system, which reconciled the activation of the laser with that of the camera, in order to obtain images of a pulse per revolution of the axis.

After going through the multicalibration procedure of Fig. 6, the dewarped images were preprocessed through the application of different filters: Gaussian (3x3 pixels kernel, 0.3 standard deviation); subtraction by local minimum (7x7 pixels kernel) and intensity capping. Subsequently, the subtraction by local average filter was applied three times (11x11 pixels kernel) and again the Gaussian filter, but with a higher standard deviation (0.6). In PIV processing, standard cross correlation (SCC) optimized by an iterative multigrid interrogation window deformation strategy was applied from

the adjustment of the spatial resolution (Kim and Sung, 2006; Scarano, 2002). In this strategy, the processing was made in 5 steps, in which the size of the interrogation window was progressively decreased, from 48 x 48 pixels to 20 x 20 pixels, with a 25% reduction in each step and with a percentage of overlap between neighbor windows of 25% for the first four steps and 50% in the last step, resulting in a final analysis area of 10 x 10 pixels (0.37 x 0.37 mm). After each step, a simple postprocessing was applied to eliminate outliers based on the work of Westerweel and Scarano (2005). A complete postprocessing by the mean absolute deviation (MAD) method was also applied in neighborhoods of 3 x 3 interrogation windows. In this case, velocities greater than three times the MAD scale defined by Eq. 5 were considered outliers (Huber, 2004)

$$MAD = bMi(|x_i - M_i(x_i)|) \tag{5}$$

Where b is a constant equal to 1.4826, M_i is the median of the kernel and x_i is the observed variable. The outliers identified by the MAD scale were eliminated and replaced by values interpolated from a cubic spline (Fritsch and Carlson, 1980).

The turbulent kinetic energy (TKE) was estimated from Eq. 6. Considering that in PIV 2D-2C measurements the third velocity component is unknown (in tangential direction), isotropic flow was assumed for the calculation of this component. This assumption was evaluated by Khan *et al.* (2006) and Chung *et al.* (2007) and negligible deviations were found in the comparison in measurements PIV 2D-2C and PIV 2D-3C (two dimensions and three components).

$$k = \frac{3}{4}\left(\overline{u'^2} + \overline{v'^2}\right) \tag{6}$$

where $\overline{u'^2}$ and $\overline{v'^2}$ are the root mean square velocity in radial (x) e axial (y) directions, respectively. These components were calculated according to Eq. 7, for the x direction, for example (the y direction follows the same model):

$$\overline{u'^2} = \overline{(u - \bar{u})^2} \tag{7}$$

The effect of the different image distortion compensation approaches on the TKE distribution for camera 1 is shown in Figure 8. In all cases, the impeller axis was chosen as a reference for the coordinates. It was observed that there was no significant variation between the TKE distributions calculated from the images with calibration and with multi-calibration. This was more evident when assessing the TKE profile at y = 85 mm (Figure 9) and x = 57 mm (Figure 10), which correspond to the dashed lines in Figure 8. In addition to the compression of the physical space in the image plane, he observed lower TKE values calculated from distorted images, that is, images without calibration. For camera 1, the two calibration strategies are indicated if at least in the region of interest the mapping function is adjusted, that is if the reference grid is aligned with the points on the plate. In this case, multi-calibration is necessary if the region of interest is also the one close to the wall.

4. CONCLUSION

This work investigated the performance of the approach developed by Soloff *et al.* (1997) to compensate image distortions of PIV measurements in a stirred tank without using solutions in the physical space, such as wedges. In the proposed calibration, images were investigated from two cameras positioned in different perspectives, but focusing on the same plane of the object, where a mapping function for each camera was estimated through a calibration target. Besides, the distribution of turbulent kinetic energy (TKE) from dewarped images was evaluated. Based on the error of adjustment of the mapping function and the qualitative analysis of the grid overlap, the approach developed by Soloff *et al.* (1997) has shown promising for the camera positioned with the smallest angular displacement in relation to the object plane. However, only the regions close to the impeller shaft and tip have been adequately compensated. From this situation, a multicalibration was proposed to adjust the region close to the wall. Consequently, the region near the impeller shaft was distorted. However, analyzing the distribution of TKE, the calibration and the multicalibration did not present significant differences, consequently, both were considered adequate in the analysis of stirred tanks.

5. ACKNOWLEDGEMENTS

This study was financed by Petrobras S/A (process number 2017/00376-1) and National Council for Scientific and Technological Development (CNPq; process numbers 142604/2019-4 and 140997/2019-9).

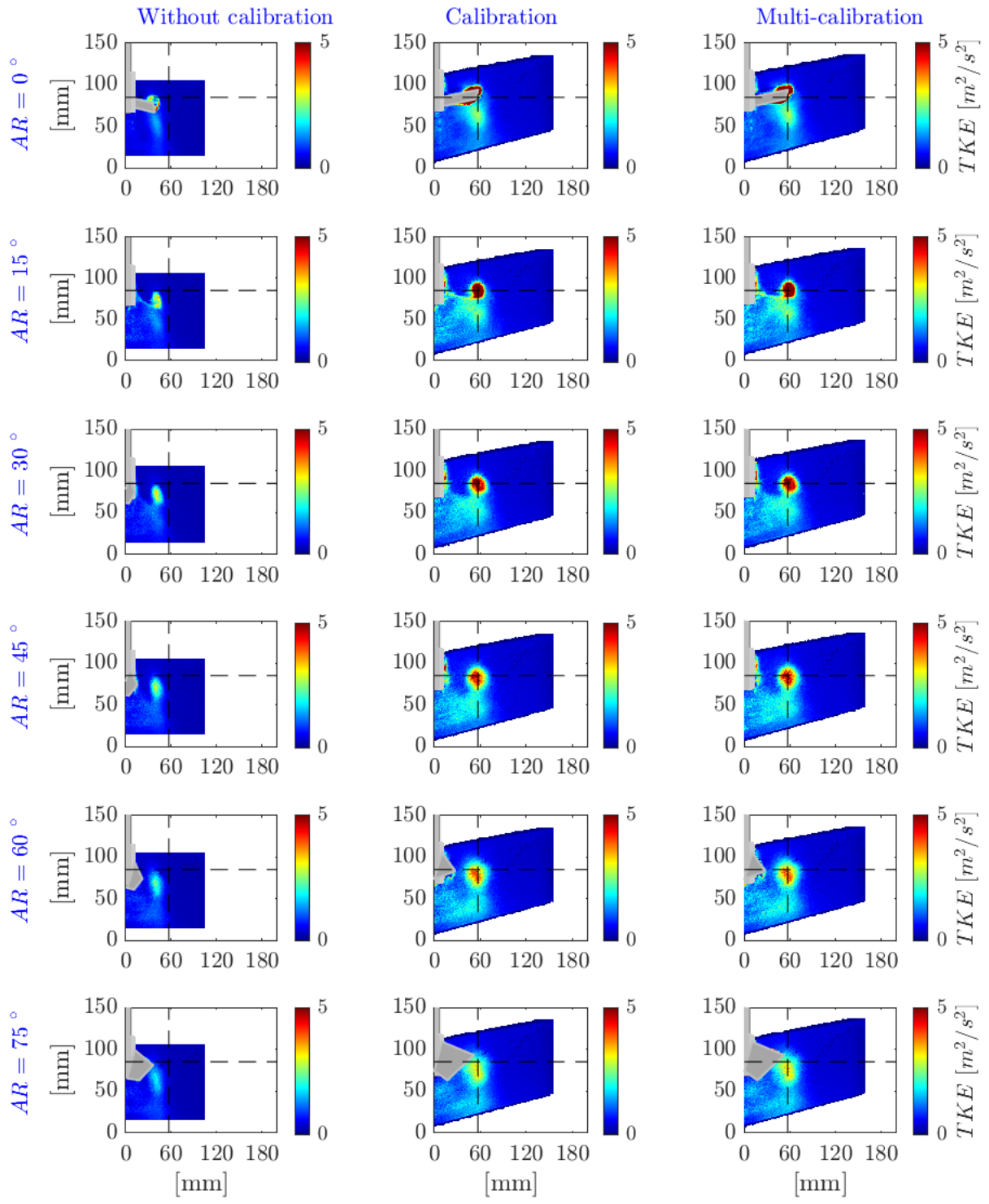

Figure 8. Turbulent kinetic energy distribution for images from camera 1 without calibration, with the calibration of Soloff *et al.* (1997) and with multicalibration.

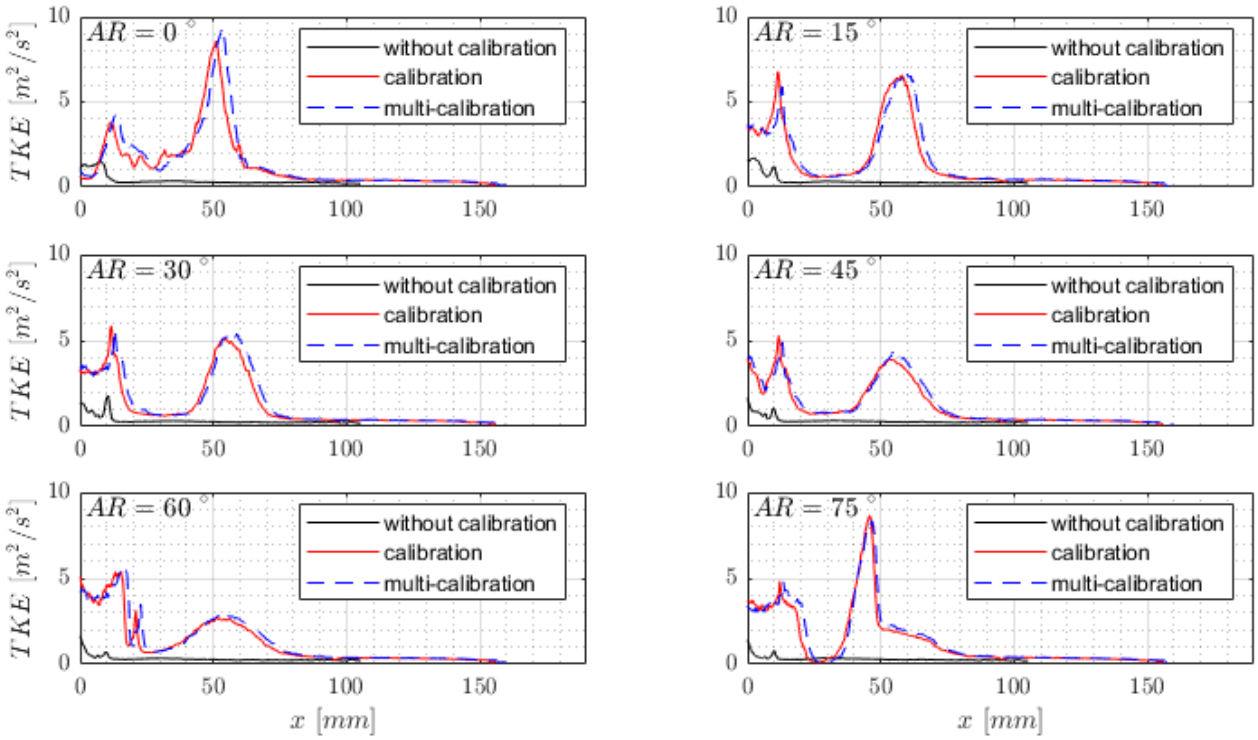

Figure 9. Effect of different image distortion compensation approaches on the profile of turbulent kinetic energy as a function of the horizontal position for camera 1 and y = 85 mm.

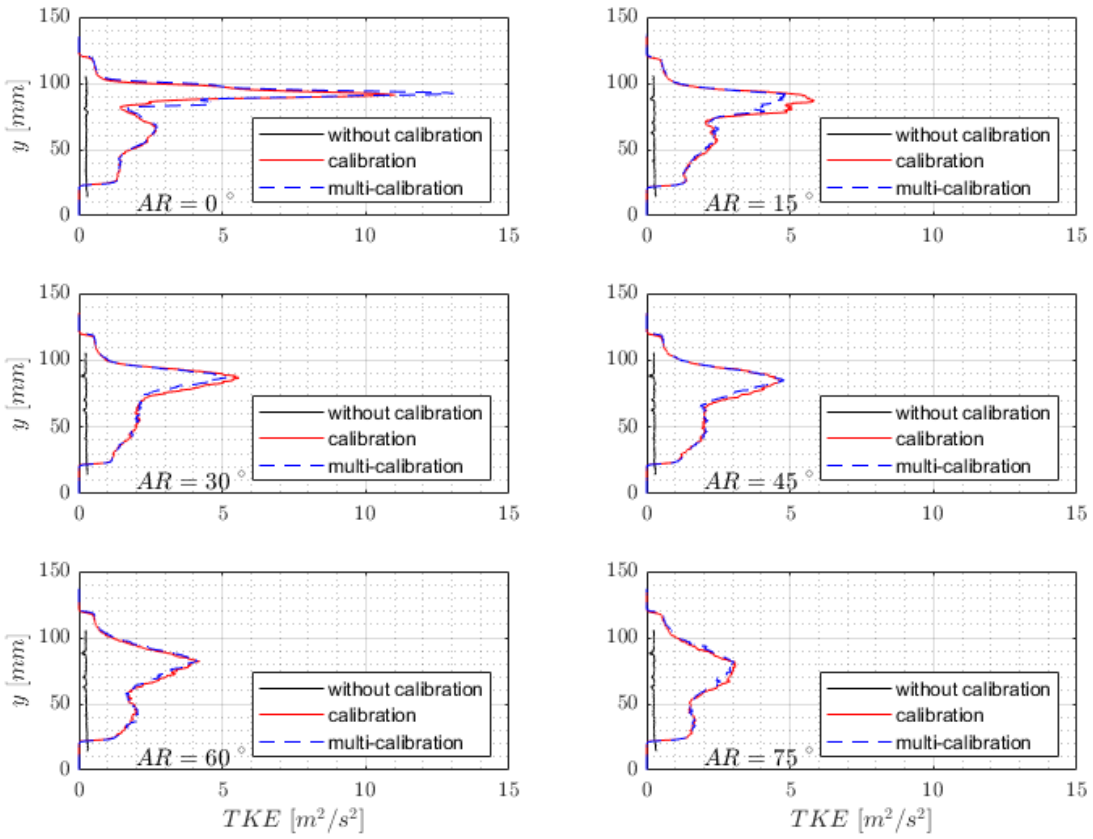

Figure 10. Effect of different image distortion compensation approaches on the profile of turbulent kinetic energy as a function of the vertical position for camera 1 and x = 57 mm.

6. REFERENCES

Adrian, R. J. and Westerweel, J., 2011. *Particle Image Velocimetry*. Cambridge University Press, New York, 1st edition.

Alberini, F., Liu, L., Stitt, E. H. and Simmons, M. J. H., 2017. Comparison between 3-D-PTV and 2-D-PIV for determination of hydrodynamics of complex fluids in a stirred vessel. *Chemical Engineering Science*, Vol. 171, p. 189–203.

Alonzo-Garcia, A., Mendoza-Escamilla, V. X., Martinez-Delgadillo, S. A., Gonzalez-Neria, I., Del C Gutiérrez-Torres, C. and Jiménez-Bernal, J. A., 2019. On the performance of different rans based models to describe the turbulent flow in an agitated vessel using non-structured grids and PIV validation. *Brazilian Journal of Chemical Engineering*, Vol. 36(1), p. 361–382.

Chung, K. H.K., Barigou, M. and Simmons, M. J. H., 2007. Reconstruction of 3-D flow field inside miniature stirred vessels using a 2-D PIV technique. *Chemical Engineering Research and Design*, Vol. 85(5A), 560–567.

Chung, Kenneth H.K., Simmons, M. J. H. and Barigou, M., 2009. Angle-resolved particle image velocimetry measurements of flow and turbulence fields in small-scale stirred vessels of different mixer configurations. *Industrial and Engineering Chemistry Research*, Vol. 48(2), p. 1008–1018.

de Lamotte, A., Delafosse, A., Calvo, S., Delvigne, F. and Toye, D., 2017. Investigating the effects of hydrodynamics and mixing on mass transfer through the free-surface in stirred tank bioreactors. *Chemical Engineering Science*, Vol. 172, p. 125–142.

Elsinga, G. E., Van Oudheusden, B. W. and Scarano, F., 2005. Evaluation of aero-optical distortion effects in PIV. *Experiments in Fluids*, Vol. 39(2), p. 246–256.

Escudié, R. and Liné, A., 2003. Experimental analysis of hydrodynamics in a radially agitated tank. *AIChE Journal*, Vol. 49(3), p. 585–603.

Fang, J., Ling, X. and Sang, Z. F., 2011. Experimental and Numerical Studies of the Flow Field in a Stirred Tank Equipped with Multiple Side-Entering Agitators. *Chemical Engineering and Technology*, Vol. 34(10), p. 1619–1629.

Fritsch, F. N., and Carlson, R. E. (1980). Monotone Piecewise Cubic Interpolation. *SIAM Journal on Numerical Analysis*, Vol 17(2), p. 238–246.

Gómez, C., Bennington, C. P. J. and Taghipour, F., 2010. Investigation of the flow field in a rectangular vessel equipped with a side-entering agitator. *Journal of Fluids Engineering, Transactions of the ASME*, Vol 132(5), p. 0511061–13.

Huber, P. J., 2004. Scale Estimates. In *Robust Statistics* (p. 107–126). John Wiley and Sons, Inc, Hoboken, 1st edition.

Khan, F. R., Rielly, C. D., and Brown, D. A. R., 2006. Angle-resolved stereo-PIV measurements close to a down-pumping pitched-blade turbine. *Chemical Engineering Science*, Vol. 61(9), p. 2799–2806.

Kilander, J., and Rasmuson, A. (2005). Energy dissipation and macro instabilities in a stirred square tank investigated using an le PIV approach and LDA measurements. *Chemical Engineering Science*, *60*(24), 6844–6856.

Kim, B. J. and Sung, H. J., 2006. A further assessment of interpolation schemes for window deformation in PIV. *Experiments in Fluids*, Vol. 41(3), p. 499–511.

Kresta, S. M. and Wood, P. E., 1991. Prediction of the three-dimensional turbulent flow in stirred tanks. *AIChE Journal*, Vol. 37(3), p. 448–460.

Li, Z., Bao, Y. and Gao, Z., 2011. PIV experiments and large eddy simulations of single-loop flow fields in Rushton turbine stirred tanks. *Chemical Engineering Science*, Vol. 66(6), p. 1219–1231.

Micheletti, M., Baldi, S., Yeoh, S. L., Ducci, A., Papadakis, G., Lee, K. C., and Yianneskis, M. (2004). On spatial and temporal variations and estimates of energy dissipation in stirred reactors. *Chemical Engineering Research and Design*, Vol. 82(9 - special issue), p. 1188–1198.

Prasad, A. K., 2000. Stereoscopic particle image velocimetry. *Experiments in Fluids*, Vol. 29(2), p. 103–116.

Prasad, Ajay K., and Jensen, K., 1995. Scheimpflug stereocamera for particle image velocimetry in liquid flows. *Applied Optics*, p. 34(30), p. 7092-7099.

Raffel, M., Willert, C. E., Scarano, F., Kähler, C. J., Wereley, S. T. and Kompenhans, J., 2018. *Particle Image Velocimetry*. Springer International Publishing, Cham, 3rd edition.

Scarano, F., 2002. Iterative image deformation methods in PIV. *Measurement Science and Technol*, Vol. 13(13), p. 1–19.

Sharp, K. V. and Adrian, R. J., 2001. PIV Study of small-scale flow structure around a Rushton turbine. *AIChE Journal*, Vol. 47(4), p. 766–778.

Soloff, S. M., Adrian, R. J. and Liu, Z. C., 1997. Distortion compensation for generalized stereoscopic particle image velocimetry. *Measurement Science and Technology*, Vol. 8(12), p. 1441–1454.

Stelmach, J., Musoski, R., Kuncewicz, C. and Głogowski, M., 2019. Turbulent energy dissipation rate and turbulence scales in the blade region of a self-aspirating disk impeller. *Journal of Applied Fluid Mechanics*, Vol. 12(3), p. 715–728.

Westerweel, J. and Scarano, F., 2005. Universal outlier detection for PIV data. *Experiments in Fluids*, Vol. 39(6), p 1096–1100.

Wieneke, B. (2005). Stereo-PIV using self-calibration on particle images. *Experiments in Fluids*, Vol. 39(2), p. 267–280.

Wieneke, B., 2017. *PIV Uncertainty Quantification and Beyond*. Ph.D thesis. Delft University of Technology, Delft. <https://doi.org/https://doi.org/10.4233/uuid:4ca8c0b8- 0835-47c3-8523-12fc356768f3>.